International Journal of Solids and Structures 46 (2009) 3451–3462

Contents lists available at ScienceDirect

International Journal of Solids and Structures

journal homepage: www.elsevier.com/locate/ijsolstr

Bending of a poroelastic beam with lateral diffusion

George W. Scherer *, Jean H. Prévost, Zhi-Hua Wang

Dept. Civil & Env. Eng., Eng. Quad. E-319, Princeton University, Princeton, NJ 08544, USA

ARTICLE INFO

Article history:
Received 17 February 2009
Received in revised form 27 May 2009
Available online 6 June 2009

Keywords:
Stress relaxation
Beams and columns
Porous material
Strain compatibility
Finite elements

ABSTRACT

Bending an elastic beam leads to a complicated 3D stress distribution, but the shear and transverse stresses are so small in a slender beam that a good approximation is obtained by assuming purely uniaxial stress. In this paper, we demonstrate that the same is true for a saturated poroelastic beam. Previous studies of poroelastic beams have shown that, to satisfy the Beltrami–Michell compatibility conditions, it is necessary to introduce either a normal transverse stress or shear stresses in addition to the bending stress. The problem is further complicated if lateral diffusion is permitted. In this study, a fully coupled finite element analysis (FEA) incorporating the lateral diffusion effect is presented. Results predicted by the "exact" numerical solution, including load relaxation, pore pressure, stresses and strains, are compared to an approximate analytical solution that incorporates the assumptions of simple beam theory. The applicability of the approximate beam-bending solution is investigated by comparing it to FEA simulations of beams with various aspect ratios. For "beams" with large width-to-height ratios, the Poisson effect causes vertical deflections that cannot be neglected. It is suggested that a theory of plate bending is needed in the case of poroelastic media with large width-to-height ratios. Nevertheless, use of the approximate solution yields very small errors over the range of width-to-height ratios (*viz.*, 1–4) explored with FEA.

1. Introduction

Poroelastic analysis of bending beams and plates is of interest for problems ranging from geomechanics to biomechanics, so several approximate solutions have been proposed (Corfdir and Dormieux, 1998; Nowinski and Davis, 1972; Zhang and Cowin, 1994; Kameo et al., 2008; Cheng, 1998; Li et al., 1995; Cederbaum et al., 1998; Taber, 1992; Wang et al., 2009). To the authors' knowledge, no exact 3D solution of the bending problem is currently available. Indeed, exact solutions are rare in poromechanics, and are usually restricted to 2D problems (*e.g.*, Mandel, 1953; Cryer, 1963; Chen, 1966). It is the purpose of this paper to assess the accuracy of a simplified solution for the beam-bending problem proposed by Scherer (1992, 2000, 2004), in which the strain field is assumed to agree with simple bending theory. This leads to simple expressions for the stresses and strains that are used in the diffusion equation to solve for the pore pressure during three-point bending. The motivation for the analysis was to determine the permeability of the beam by measuring the kinetics of relaxation of the vertical reaction force during constant deflection or constantly increasing deflection. Measurements were found to be in excellent agreement with the theory (*e.g.*, Scherer, 1992, 1996; Vichit-Vadakan and Scherer, 2000; Valenza and Scherer, 2004), in spite of its obvious theoretical deficiencies. The purpose of the present paper is to compare the approximate analysis of a rectangular beam to a fully coupled finite element analysis (FEA) performed using Dynaflow® (Prévost, 1981). A similar comparison between FEA and the analytical solution by Zhang and Cowin (1994) was performed by Manfredini et al. (1999), and good agreement was found. However, that analysis was performed in what we call the "rigid limit" (defined below), where the impact of the pore fluid is relatively small, so discrepancies between the analytical and exact solutions are expected to be small. In our simulations, we will work in the "gel limit", where the pore fluid is dominant and the errors caused by approximations are accentuated.

2. Problem definition

2.1. Constitutive relation

In linear poroelasticity theory, assuming zero initial stress and pore pressure, Biot's constitutive equations can be expressed by (Biot, 1941; Rice and Cleary, 1976)

$$\sigma_{ij} = \left(K - \frac{2}{3}G\right)\varepsilon\delta_{ij} + 2G\varepsilon_{ij} - bp_f\delta_{ij} \tag{1}$$

where ε_{ij} and σ_{ij} are linear strain and total stress tensors, respectively, δ_{ij} the Kronecker delta, K and G the bulk and shear moduli of the drained porous matrix, $\varepsilon = \varepsilon_{kk}$ the volumetric strain, p the

* Corresponding author. Tel.: +1 6092585680; fax: +1 6092581563.
E-mail address: scherer@princeton.edu (G.W. Scherer).

0020-7683/$ - see front matter © 2009 Elsevier Ltd. All rights reserved.
doi:10.1016/j.ijsolstr.2009.05.016

fluid pore pressure, and $b = 1 - K/K_s$ the Biot's coefficient, with K_S the bulk modulus of the solid phase and subscript '*s*' denoting the properties of the solid grains. Alternatively, the linear strain tensor can be expressed in terms of the total stress:

$$\varepsilon_{ij} = \frac{1+v}{E}(\sigma_{ij} + bp_f\delta_{ij}) - \frac{3v}{E}(\sigma + bp_f)\delta_{ij} \tag{2}$$

where E is the Young's modulus and v the Poisson's ratio of the drained porous body and $\sigma = \sigma_{kk}/3$ is the mean normal stress.

2.2. Field equations

The continuity equation of a compressible fluid inside a saturated porous medium is

$$\frac{d(\phi\rho_f)}{dt} + \nabla\cdot\left(\rho_f \underset{\sim}{q_f}\right) = 0 \tag{3}$$

where subscript '*f*' denotes properties of the fluid, ϕ is the Lagrangian porosity, and $\underset{\sim}{q_f}$ is the fluid flux or filtration vector defined by Darcy's law

$$\underset{\sim}{q_f} = -\kappa\left(\nabla p_f - \rho_f \underset{\sim}{g}\right) \tag{4}$$

where g is the body force vector and $\kappa \equiv k/\mu$ is the mobility, with k the permeability of the porous matrix, and μ the viscosity of the fluid.

The Lagrangian porosity, ϕ, is related to the more commonly used Eulerian porosity, φ, by (see *e.g.*, Coussy, 2004)

$$\phi = \varphi \det \underset{\sim}{F} \tag{5}$$

where $\underset{\sim}{F}$ = solid deformation gradient. Porosity and fluid mass density are given by the following:

$$\phi - \phi_0 = b\nabla\cdot\underset{\sim}{u^S} + \frac{b-\phi_0}{K_S}p_f \tag{6}$$

$$\frac{\rho_f - \rho_f^0}{\rho_f^0} = \frac{p_f}{K_f} \tag{7}$$

where the subscript/superscript 0 denotes the initial values, u^S is the 3D solid displacement field, and K_f is the bulk modulus of the pore fluid.

Without body force, the resulting diffusion equation can be derived from the fluid continuity equation, the momentum balance equation, and Biot's constitutive relation as (see *e.g.*, Coussy, 2004)

$$c_f\nabla^2\left(\sigma_{kk} + \frac{3}{B}p_f\right) = \frac{\partial}{\partial t}\left(\sigma_{kk} + \frac{3}{B}p_f\right) \tag{8}$$

where c_f is the diffusivity coefficient defined by (Coussy, 2004; Rice and Cleary, 1976):

$$c_f = \kappa\left[\frac{2(1-v)G}{(1-2v)}\right]\left[\frac{B^2(1-2v)(1+v_u)^2}{9(v_u-v)(1-v_u)}\right] \tag{9}$$

and B is Skempton's coefficient defined by (Skempton, 1954)

$$B = \frac{bM}{K + b^2M} \tag{10}$$

where the Biot modulus, M, is defined by

$$\frac{1}{M} = \frac{b-\phi_0}{K_S} + \frac{\phi}{K_f} \tag{11}$$

The Skempton coefficient is a measure of the relative compressibility between solid and fluid. The term v_u is the undrained Poisson's ratio defined by

$$v_u = -\left.\frac{d\varepsilon_{jj}}{d\varepsilon_{ii}}\right|_{dm_f=dT=d\sigma_{ii}=0} = \frac{3v + B(1-2v)b}{3 - B(1-2v)b} \quad i\neq j \tag{12}$$

with $-1 < v < v_u \leqslant 0.5$.

To guarantee the existence of a single-valued displacement field by solving stress/strain equations, it is necessary for the coupling of stresses and pore pressure to satisfy the Beltrami–Michell compatibility equations (Rice and Cleary, 1976; Detournay and Cheng, 1994; Coussy, 2004)

$$\nabla^2\left[(1+v)\sigma_{ij} - v\sigma_{kk}\delta_{ij}\right] + \frac{\partial^2\sigma_{kk}}{\partial x_i\partial x_j} + b(1-2v)\left[\nabla^2 p_f\delta_{ij} + \frac{\partial^2 p_f}{\partial x_i\partial x_j}\right] = 0 \tag{13}$$

A contracted form of Eq. (13) is obtained by setting $i = j$, as

$$\nabla^2(\sigma_{kk} + \Lambda p_f) = 0 \tag{14}$$

where

$$\Lambda = \frac{2b(1-2v)}{(1-v)} = \frac{6(v_u - v)}{B(1+v_u)(1-v)} \tag{15}$$

2.3. Boundary conditions

As discussed in detail in Wang et al. (2009), deriving a complete analytical solution to the general beam-bending problem proves to be analytically intractable. In particular, it was shown that even for the simpler pure bending problem, the solution cannot be resolved analytically in the absence of shear stresses when traction-free boundary conditions on both horizontal and lateral faces must be enforced. In Wang et al. (2009), an approximate solution was derived under the simplified assumption that traction-free conditions on the lateral faces are satisfied in the St. Venant's sense, as earlier assumed by Zhang and Cowin (1994). However, the resulting solution was shown to be somewhat deficient. In this paper, we use another simplified analysis and assess its accuracy.

Consider a poroelastic beam, $-L < x < L$, $-c < y < c$, and $-a < z < a$, as shown in Fig. 1, subjected to a point load P in the middle. Due to symmetry, we only need to consider half of the

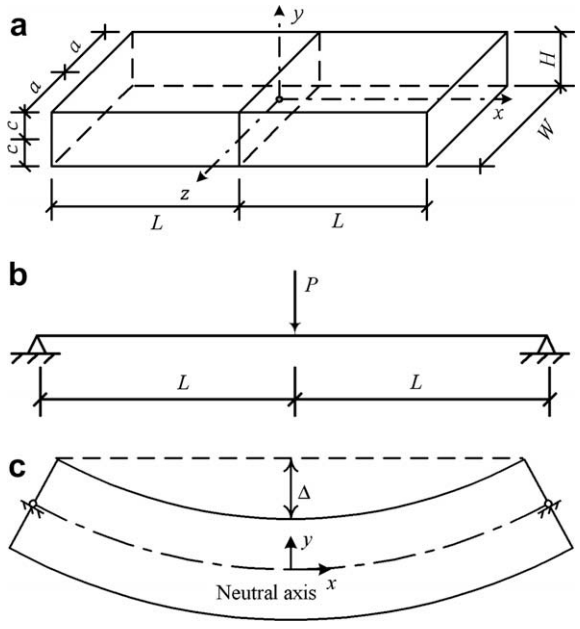

Fig. 1. Bending of poroelastic beam: (a) dimensions of the 3D model; (b) three-point bending scheme; and (c) the longitudinal section.

beam span, $0 < x < L$ and width, $0 < z < a$. To derive the analytical solution, the following pressure, stress and displacement boundary conditions are considered. Fluid is drained through the top and bottom surfaces of the beam, as well the lateral surfaces, so

$$p_f(x,\ y = \pm c,\ z,\ t) = 0, \quad p_f(x,\ y,\ z = \pm a,\ t) = 0 \tag{16}$$

This is different from the problem setting in Wang et al. (2009), in that here we allow lateral diffusion. Accordingly, solutions of pore pressure and stresses have the additional spatial dependence on z.

The ratio between the shear stress and the bending stress for a beam subjected to three-point bending is approximately given by (Timoshenko, 1940)

$$\left|\frac{\tau_{xy}}{\sigma_x}\right| = \frac{(c^2 - y^2)}{2(L-x)y} \tag{17}$$

and

$$\frac{\tau_{xy,\max}}{\sigma_{x,\max}} = \frac{1}{2}\left(\frac{c}{L}\right) \tag{18}$$

Thus for sufficiently long beams (*i.e.* the aspect ratio $c/L << 1$), the in-plane shear stress τ_{xy} is negligible. The presence of transverse stress in the three-point bending scheme shown in Fig. 1(b) is mainly due to the presence of both the shear stresses and undrained pore fluid, and is of the same order of magnitude as τ_{xy}, so it is also negligible. Therefore, as a reasonable approximation based on beam theory, the only non-vanishing stress is the bending stress σ_x:

$$\sigma_y = \sigma_z = 0, \quad \tau_{xy} = \tau_{yz} = \tau_{xz} = 0 \tag{19}$$

A rigorous solution of the beam-bending problem would have to include these stresses, because they have an influence on the strains that enter into the Beltrami–Michell conditions. Satisfying those conditions while ignoring these stresses, as is usually done (Wang et al., 2009), is inconsistent, and is probably responsible for the inaccuracy of the resulting solutions. However, from the FEA results we will demonstrate that the neglected strains are small, and have a minor effect on the relaxation kinetics.

The displacement boundary conditions are:

(1) Symmetry boundary condition at the midpoint of the beam, $x = 0$:

$$u(x = 0,\ y,\ z) = 0, \quad \left.\frac{\partial v}{\partial x}\right|_{x=0} = 0 \tag{20}$$

(2) No vertical deflection at the support at $x = L,\ y = 0$ and constant deflection at the midpoint, $x = 0,\ y = 0$:

$$v(x = L,\ y = 0,\ z) = 0, \quad v(x = 0,\ y = 0,\ z) = \Delta \tag{21}$$

3. Analytical solutions for the diffusion equation

In this section, the approximate analytical solution for three-point bending, derived by Scherer (1992, 2000, 2004), is presented. The continuity equation is written as

$$\frac{\dot{p}_f}{M} + b\dot{\varepsilon} = \kappa\nabla^2 p_f \tag{22}$$

where ε is the volumetric strain and the superscript dot indicates a partial derivative with respect to time. For the bending problem, the strains are very small, so the porosity does not change significantly; therefore, $\phi \approx \phi_0$ throughout. The essential simplification in this treatment is that the strains are the same as for a non-porous elastic beam in pure bending, so we begin with the assumption that the axial strain is (Popov, 1968)

$$\varepsilon_x = \frac{3\Delta y}{L^3}(L - x) \tag{23}$$

Assuming that $\sigma_y = \sigma_z = 0$, Eq. (2) indicates that the axial stress is (Scherer, 2000)

$$\sigma_x = E\varepsilon_x - (1 - 2\nu)bp_f \tag{24}$$

Summing the strains in Eq. (2), the corresponding volumetric strain is

$$\varepsilon = \frac{\sigma_x + 3bp_f}{3K} = (1 - 2\nu)\varepsilon_x + \frac{2(1+\nu)bp_f}{3K} \tag{25}$$

Substituting Eqs. (23) and (25) into Eq. (22) leads to a tractable equation for the pore pressure.

The pressure obtained in this way is obviously not rigorous, because, as we shall see, the resulting strains do not satisfy the Beltrami–Michell equations; moreover, the relaxation kinetics are described by an unconventional diffusivity coefficient (Scherer, 1992, 2000, 2004):

$$\frac{1}{c_{fu}} = \frac{1}{\kappa}\left(\frac{\phi}{K_f} + \frac{b - \phi}{K_S} + \frac{2(1+\nu)b^2}{3K}\right) \tag{26}$$

(or, in the notation of (Scherer, 2004), $c_{fu} = a^2/\tau_R$). In the gel limit ($K << K_f$ and $K << K_S$), this reduces to

$$c_{fu} = \frac{1}{2}\frac{E\kappa}{(1+\nu)(1-2\nu)} \tag{27}$$

On the other hand, at the gel limit, the diffusivity in Eq. (9) reduces to

$$c_f = (1 - \nu)\frac{E\kappa}{(1+\nu)(1-2\nu)} \tag{28}$$

Let $\tau = c_f t/c^2$ denote the dimensionless time. Comparing the diffusivities in Eqs. (27) and (28), we find that they differ by a factor of $2(1 - \nu)$ at the gel limit:

$$\frac{\tau_u}{\tau} = \frac{c_{fu}}{c_f} = \frac{1}{2(1-\nu)} \tag{29}$$

At the other extreme, consider a system in which the pore liquid is much more compressible than the solid phase or the porous body ($K_S > K >> K_f$). In the "rigid limit", both diffusivities reduce to

$$c_f \approx c_{fu} \approx \frac{\kappa K_f}{\phi} \tag{30}$$

Thus, in the rigid limit, the diffusivity coefficient in (Coussy, 2004) and the one in Scherer (1992, 2000, 2004) tend to approach each other. Since the gel limit represents the worst case, where error in the approximate solution is most significant, we will compare the numerical solution to the approximation in that limit. The agreement between the analytical solution and the FEA result is found to be improved compared to previous treatments (Zhang and Cowin, 1994; Wang et al., 2009; Manfredini et al., 1999) for poroelastic beams with compressible constituents.

3.1. Load relaxation

The load relaxation function predicted by the approximate solution is given by:

$$\frac{P(\tau_u)}{P^0} = \frac{1+\nu}{1+\nu_u} + \frac{\nu_u - \nu}{1+\nu_u}S_1(\tau_u)S_2\left(\frac{c}{a},\ \tau_u\right) \tag{31}$$

where superscript '0' denotes the properties at time $t = 0^+$. Since the prescribed vertical deflection Δ is invariant with time, as the fluid drains out of the beam, the applied load P required to hold

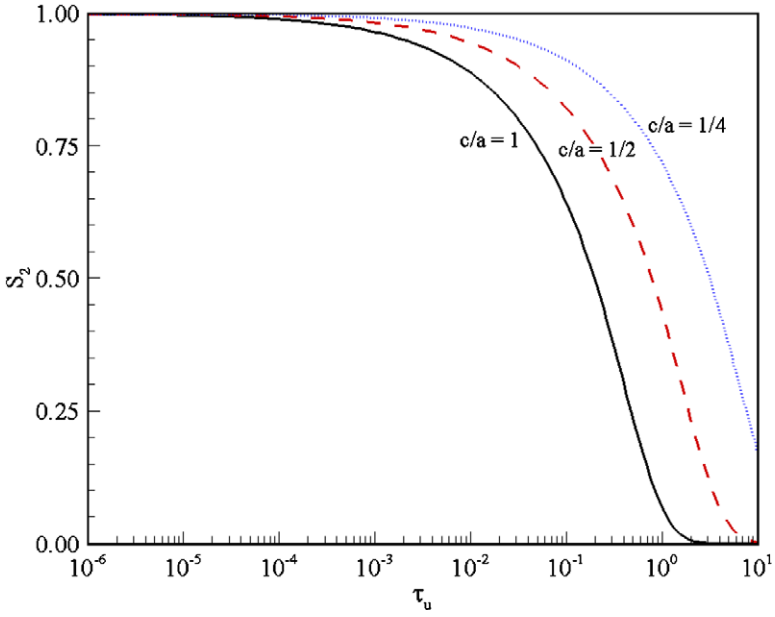

Fig. 2. Relaxation from lateral diffusion versus dimensionless time for various aspect ratios, c/a.

the constant deflection of the beam decays with time. The two time series in Eq. (31) are defined as

$$S_1(\tau_u) = \sum_{m=1}^{\infty} \frac{6}{a_m^2} \exp\left(-a_m^2 \tau_u\right), \quad a_m = m\pi \tag{32}$$

$$S_2\left(\frac{c}{a},\ \tau_u\right) = \sum_{n=1}^{\infty} \frac{2}{b_n^2} \exp\left(-b_n^2 \frac{c^2}{a^2} \tau_u\right), \quad b_n = \frac{2n-1}{2}\pi \tag{33}$$

A plot of $S_2(c/a,\ \tau_u)$ as a function of dimensionless time is shown in Fig. 2. The function $S_2(c/a,\ \tau_u) = 1$ for $a \to \infty$ or $t = 0$, so the lateral diffusion vanishes for an infinitely wide beam and at the moment of deflection of a finite beam.

3.2. Pore pressure, stresses and bending strain

The analytical solution for the pore pressure from the approximate diffusion equation is given by:

$$p_f(x,\ y,\ z,\ \tau_u) = p_0(x)p_1(y,\ \tau_u)p_2(z,\ \tau_u) \tag{34}$$

where

$$p_0(x) = -\left(\frac{Eb\Delta c}{\psi L^3}\right)(L - x) \tag{35}$$

$$p_1(y, \tau_u) = -2\sum_{m=1}^{\infty} \frac{(-1)^m}{a_m} \sin\left(a_m \frac{y}{c}\right) \exp\left(-a_m^2 \tau_u\right) \tag{36}$$

$$p_2(z, \tau_u) = -2\sum_{n=1}^{\infty} \frac{(-1)^n}{b_n} \cos\left(b_n \frac{z}{a}\right) \exp\left(-b_n^2 \frac{c^2}{a^2} \tau_u\right) \tag{37}$$

$$\psi = \frac{\phi K}{K_f} + \frac{(b-\phi)K}{K_s} + \frac{2(1+\nu)b^2}{3} \tag{38}$$

Note that the spatial variables in Eq. (34) are separable. Normal strains are given by

$$\varepsilon_y = \varepsilon_z = -\nu\varepsilon_x + \frac{(1+\nu)(1-2\nu)bp_f}{E} \tag{39}$$

The bending strain is independent of the lateral direction z and time, (*viz.*, $\dot{\varepsilon}_x = 0$). The non-vanishing bending stress is given by Eq. (24). All the other stress components vanish, as indicated in Eq. (19).

4. Results for square beams

In this section, the accuracy of the analytical solution presented in Section 3 is assessed by comparison to simulations done using FEA. The finite element mesh for a poroelastic beam under three-point bending is shown in Fig. 3. Due to symmetry, only one quarter of the beam is simulated in the FEA (*viz.*, $0 \leqslant x \leqslant L$, $-c \leqslant y \leqslant c$, $0 \leqslant z \leqslant a$). The mesh is refined toward the location of load application, $x = 0$, and the drainage surfaces, $y = \pm c$, $z = a$.

To simulate the case in which the error of the approximation is expected to be worst, beams investigated in this study consist of incompressible constituents, with $b = 1.0$, $B = 1.0$, and $\nu_u = 0.5$. The analytical solutions are applicable to beams with compressible constituents as well. Furthermore, we assume that the porous matrix is isotropic and homogenous. The following material properties are used: $E = 10^6$ Pa, $\rho_s = 2 \times 10^3$ kg/m^3, $\rho_f = 10^3$ kg/m^3, $k = 1.6 \times 10^{-18}$ m^2, $\mu = 10^{-3}$ Pa s and $\phi = 0.95$. The dimensions of the square beam are $L = 0.1$ m, $a = c = 0.005$ m and the prescribed deflection is $\Delta = -0.0025$ m.

First, the analytical load relaxation is compared with FEA. For a square beam, typical results of comparison are shown below. Plots of the load relaxation versus dimensionless time are shown in Figs. 4 and 5 for beams with $\nu = 0$ and $\nu = 0.3$, respectively. The analytical solution is very accurate in predicting the load relaxation, in particular for large Poisson's ratio. A slight discrepancy at the initial stage of transient diffusion is observed for small Poisson's ratio. For the purpose of using the beam-bending method for measuring material permeability (Scherer, 1992), this discrepancy is insignificant.

Comparisons between the analytical solution and FEA for pore pressure, total stresses and strains for a square beam with $\nu = 0.2$ are presented below. Longitudinal, vertical and transverse pressure distributions at different dimensionless times are plotted in Figs. 6–8, respectively. In these comparisons, the dimensionless time is computed using the diffusivity coefficient in Eq. (9). It is clear that the pressure distribution along the axial direction is in very good agreement with the FEA, except for a slight discrepancy at the mid-plane $x/L = 0$. Physically we expect the pressure

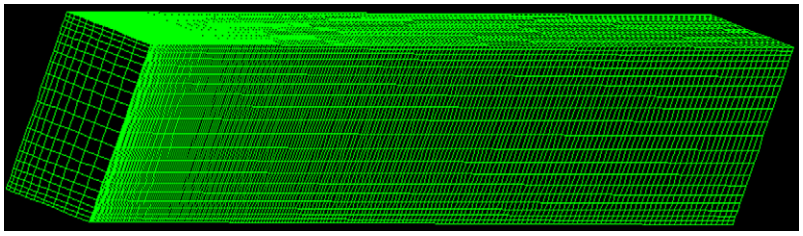

Fig. 3. Finite element mesh.

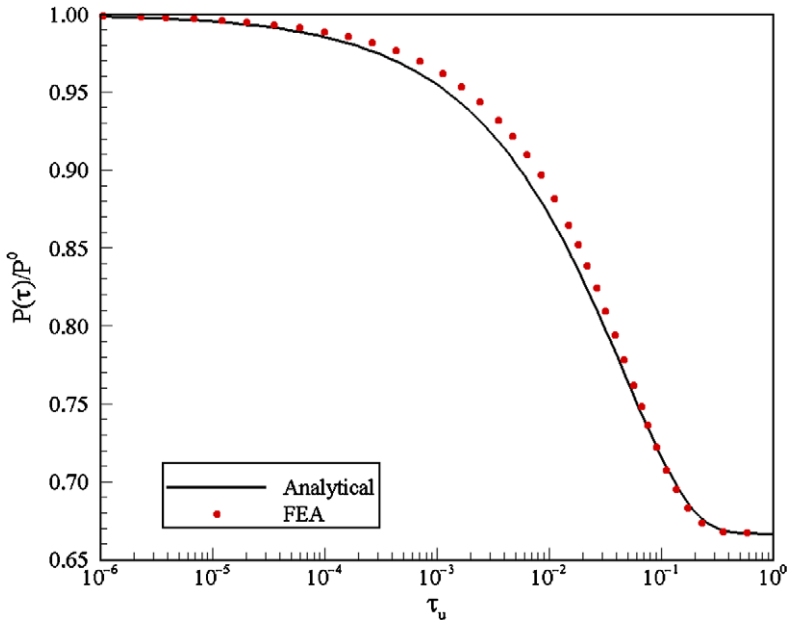

Fig. 4. Load relaxation for square beam with $\nu = \mathbf{0}$.

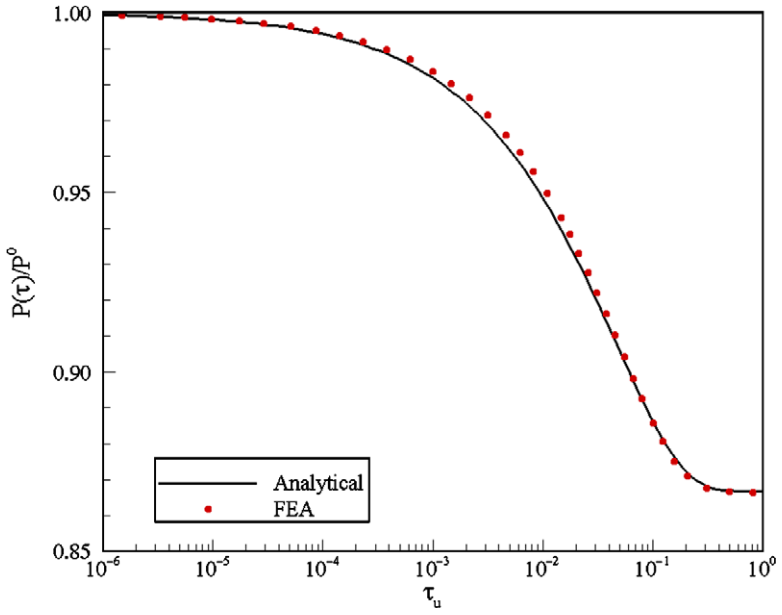

Fig. 5. Load relaxation for square beam with $\nu = 0.3$.

gradient $(\partial p/\partial x)|_{x=0} = 0$ at the mid-plane, which is observed in the FEA results in Fig. 6. On the other hand, the analytical solution of pore pressure predicts a strictly linear pressure distribution with the range $0 \leqslant x/L \leqslant 1$. Thus, in the vicinity of $x/L = 0$, it is natural to see the discrepancy of pressure distribution between the analytical solution and FEA.

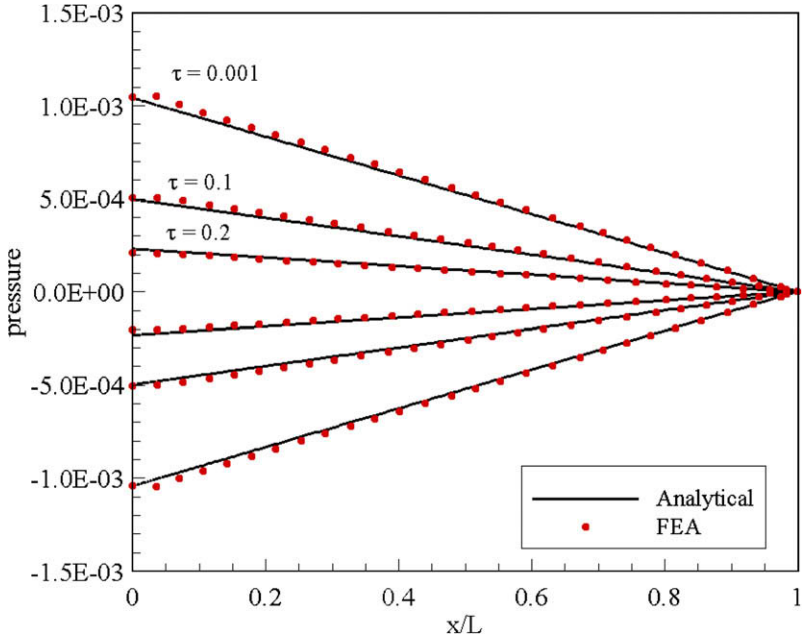

Fig. 6. Pressure along axial direction at $y/c = \pm 2/3,\ z/a = 0$. The departure from linearity is strongly localized near the center of the beam, so the linear assumption is quite accurate.

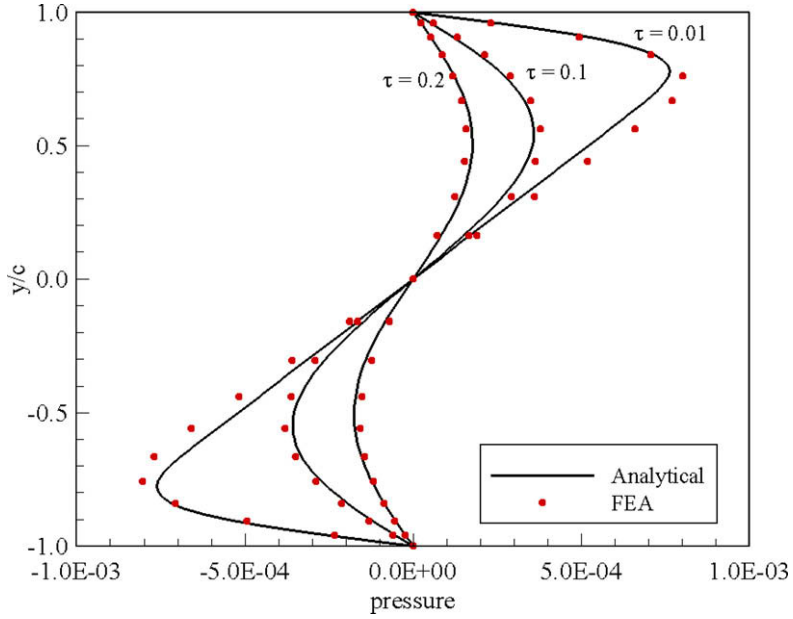

Fig. 7. Pressure along vertical direction at $x/L = 1/3,\ z/a = 0$.

The vertical pressure distribution predicted by the analytical method is reasonably accurate, except for small times. The dimensionless time for the finite element mesh is $\tau_{\text{mesh}} = c_f \Delta t / h^2$, where Δt is the FEA time step size and the characteristic finite element mesh size is $h = \sqrt{\sum_{i=1}^{nsd} \Delta x_i^2}$ with *nsd* the number of dimensions, and Δx_i the length of a finite element in the x_i direction. The value of $\tau_{\text{mesh}} = c_f \Delta t / h^2$ for the square beam was checked along all three directions, and found to be $\tau_{\text{mesh}} \sim O(10^{-2}) < 1.0$. Thus, the early discrepancy in pressure seen in Fig. 8 may result from the pore pressure oscillation in FEA for $\tau_{\text{mesh}} < 1.0$ (Vermeer and Verruijt, 1981; Thomas and Zhou, 1997), as a consequence of either small time step Δt or coarse mesh. It was shown by Truty and Zimmermann (2006) that pressure oscillations at $\tau_{\text{mesh}} < 1.0$ can be effectively suppressed by using stabilization schemes for the finite element formulation, but that was not done in the present work.

Figs. 9 and 10 show the distribution of bending stresses σ_x along horizontal and vertical directions, respectively. As the dimensionless time increases, the contribution from the pore pressure vanishes with the depletion of pore fluid, and the bending stress approaches its elastic limit (*i.e.* linearly distributed along the y axis). Even for short times, the stresses are in good agreement with the analytical solution. Similarly, the distribution of axial bending strain ε_x along horizontal and vertical directions (not shown) predicted by the analytical solution matches well with the FEA results.

FEA results for the shear stress τ_{xy} and transverse stress σ_z are plotted in Figs. 11 and 12, respectively. Comparing to Figs. 10

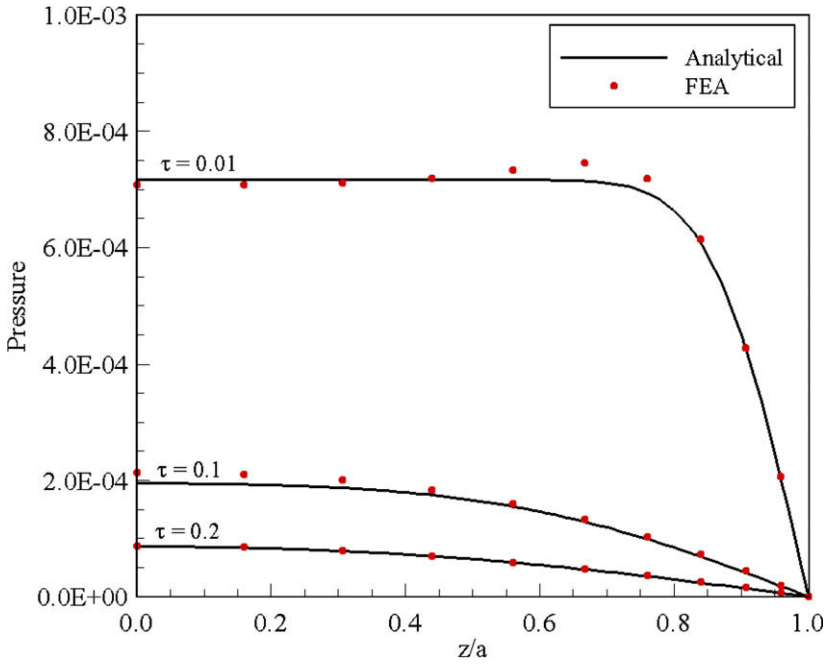

Fig. 8. Pressure along lateral direction at $x/L = 1/3,\ y/c = 0.84$. The discrepancies for $\tau = 0.01$ result from stabilization problems.

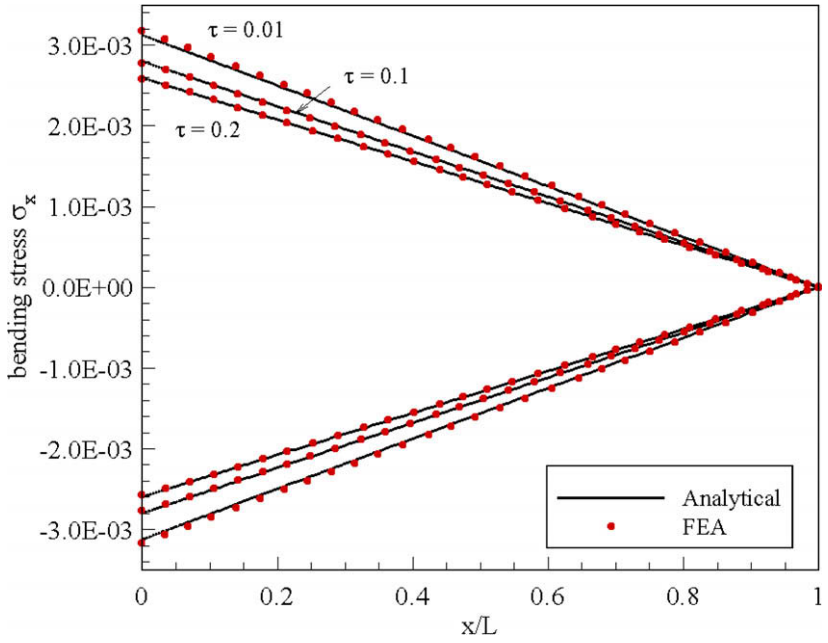

Fig. 9. Bending stress along axial direction at $y/c = \pm 2/3,\ z/a = 0$.

and 11, the ratio between the maximum shear and bending stress at $x/L = 1/3$ is $\tau_{xy}|_{x/L=1/3,y=0}/\sigma_x|_{x/L=1/3,y=c} = 1/27.6$ at $\tau = 0.2$. Using Eq. (17), at the elastic limit (*i.e.* as $\tau \to \infty$) for a poroelastic beam, we have $\tau_{xy}|_{x/L=1/3,y=0}/\sigma_x|_{x/L=1/3,y=c} = 0.75c/L \approx 1/26.7$ with $L/c = 20$. Thus, Eq. (17) is accurate in estimating the magnitude of shear stress, and it is reasonable to neglect the shear stress in the analytical solutions for beams with large L/c ratios. Fig. 12 shows that the magnitude of the transverse stress varies considerably as the fluid drainage process continues. It can vary from as little as $\sigma_{x,\max}/\sigma_{z,\max} \approx 5.0$ at $\tau = 0.01$ to $\sigma_{x,\max}/\sigma_{z,\max} \approx 25$ at $\tau = 0.2$ when diffusion is almost completed. A possible cause for the presence of relatively large transverse stresses at the initial drainage stage is suggested by the coupled diffusion Eq. (8). At $\tau = 0.01$, the fluid drainage produces a drastic rate of change of pore pressure (*cf.* Figs. 4 and 5). As the bending stress is not rate sensitive (*cf.* Fig. 10), the rate of change of pressure may be offset by the transverse stress through Eq. (8). Thus if the inclusion of time-dependent transverse stresses were mathematically tractable, the accuracy of analytical solutions could be expected to improve.

5. Effect of aspect ratios

We first investigate in this section the effect of the cross-sectional (width-to-height) ratio a/c on the predicted load relaxation

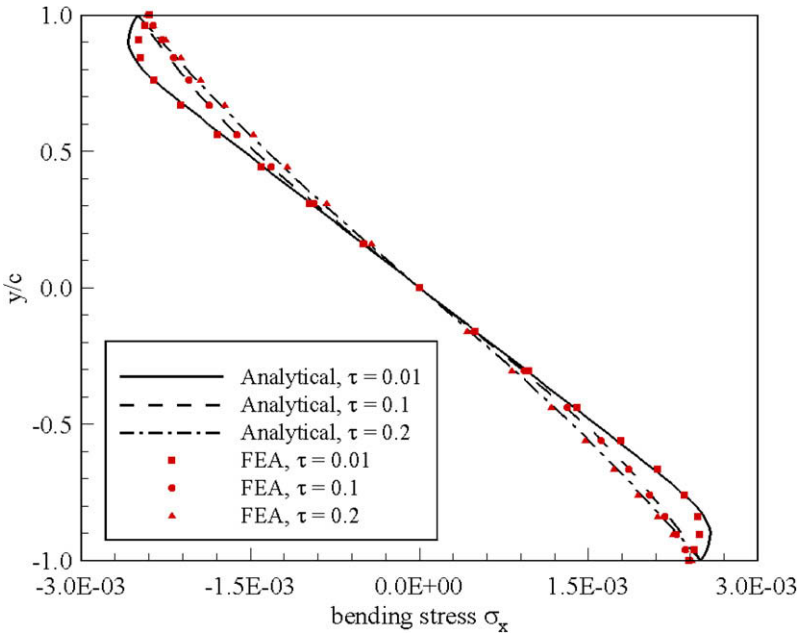

Fig. 10. Bending stress along vertical direction at $x/L = 1/3,\ z/a = 0$.

for bending of a poroelastic beam. Again, to simulate the worst case, beams with incompressible constituents and fixed Poisson's ratio $v = 0.2$ are simulated.

Load relaxation was analyzed for beams with $a/c = 0.5$, 2 and 4, respectively. For a narrow beam, the load relaxation predicted by the analytical solution is in good agreement with the FEA results, just as for the square beam. As the width-to-height ratio increases, the analytical predictions deviate from the FEA results, and tend to overestimate the asymptote as $\tau \to \infty$. The discrepancy of the limiting load relaxation ratio P^∞/P^0, where superscript '∞' denotes the properties at $\tau \to \infty$, increases with the a/c ratio, as shown in Fig. 13. The analytical solution based on beam-bending theory yields a fixed asymptote $P^\infty/P^0 = 0.8$ for beams with $v = 0.2$ and incompressible constituents. Since the asymptote P^∞/P^0 is time independent, this discrepancy cannot be corrected by improving the transient diffusion analysis.

The cause of the deficiency in the analytical solution for the large a/c results from the failure of beam theory when the width of the beam is large. Thus, we resort to plate theory to study the possible bending mechanism. For an elastic plate under pure bending moment, M, the vertical displacement was derived by Timoshenko (1940):

$$v = -\frac{M}{2EI}(x-L)^2 + \frac{vM}{2EI}z^2 \tag{40}$$

In three-point bending, we have $M(x) = P(x-L)/2$. Denoting $\Delta(z) = v(x = 0,\ z)$ at the mid-plane (y–z), we have

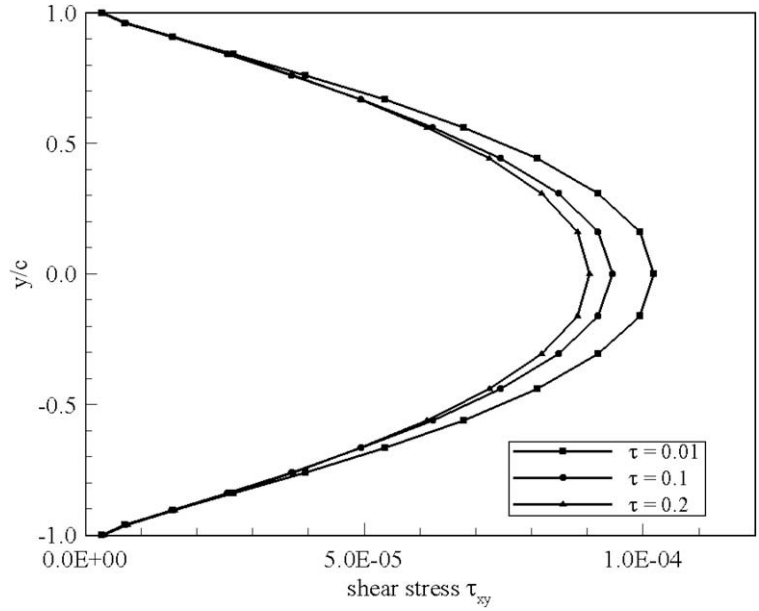

Fig. 11. Shear stress along vertical direction at $x/L = 1/3,\ z/a = 0$ from FEA.

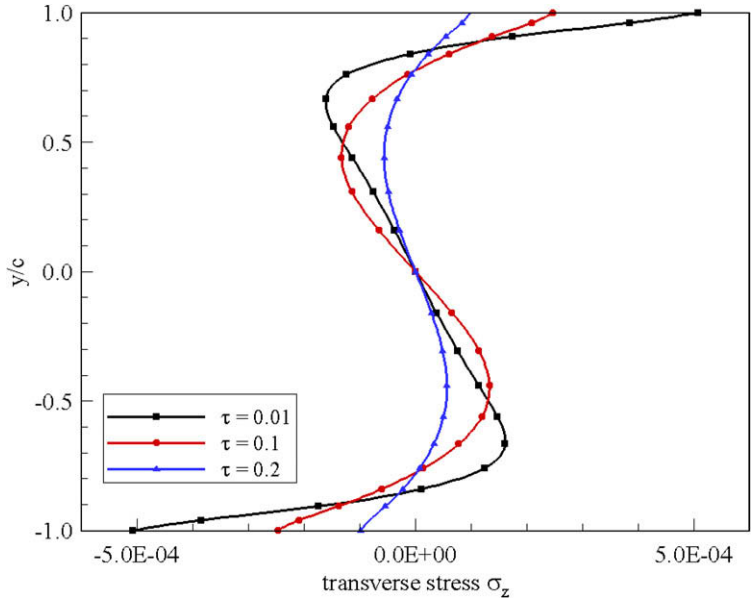

Fig. 12. Transverse stress along vertical direction at $x/L = 1/3,\ z/a = 0$ from FEA.

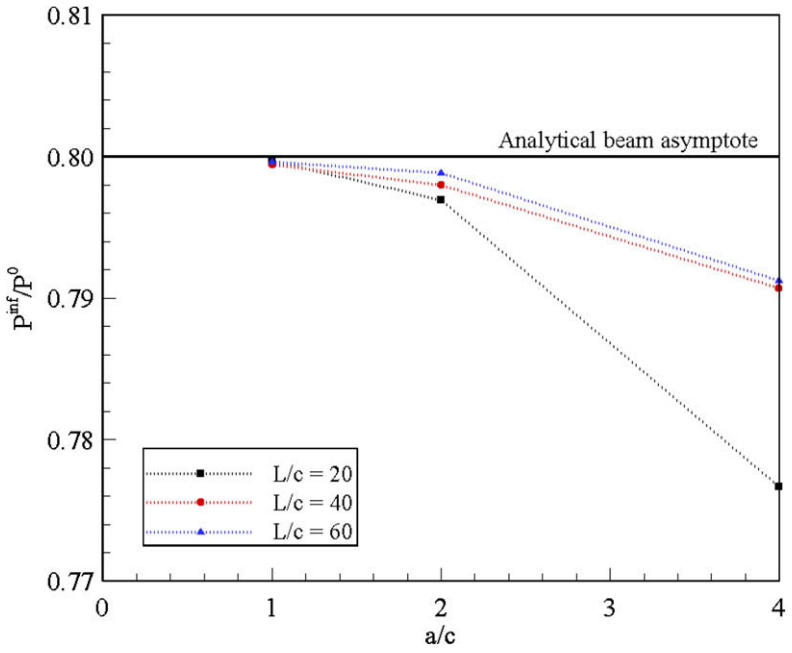

Fig. 13. Effect of aspect ratios on prediction of P^{∞}/P^{0} for beams with $v = 0.2$.

$$\Delta(z) = \frac{PL}{6EI}(L^2 - vz^2) \tag{41}$$

At the elastic limit (*i.e.* $\tau \to \infty$), the analytical solution of the vertical displacement in (Scherer, 1992, 2000, 2004) yields:

$$\Delta = \frac{PL^3}{6EI} \tag{42}$$

It is clear from Eq. (40) that, as the beam width increases, the variation of the vertical displacement v along the z direction becomes significant. On the other hand, the analytical solution using beam theory assumes a prescribed vertical displacement invariant in z. Thus, for bending of porous media with large width-to-height ratio, beam theory is no longer applicable. An analytical solution based on plate theory is therefore needed to predict the appropriate diffusion behavior. This might be obtained following Taber's method (1992), or the approach used by Scherer (1992, 2000, 2004) could be extended by assuming that the vertical deflection is described by Eq. (41).

The Poisson effect of flexure of a plate is clearly demonstrated in Fig. 14, where the vertical displacement is plotted versus the normalized z coordinate for a poroelastic plate at $x = L/3$ and $y = 0$. The Poisson's ratio is chosen to be $v = 0$, such that when the porous plate is fully drained, the Poisson's effect vanishes and the vertical displacement is invariant in z according to Eq. (41). At time $t = 0^{+}$, under a sudden displacement, the pore fluid has not yet started to escape, thus the porous plate is considered to be undrained with an

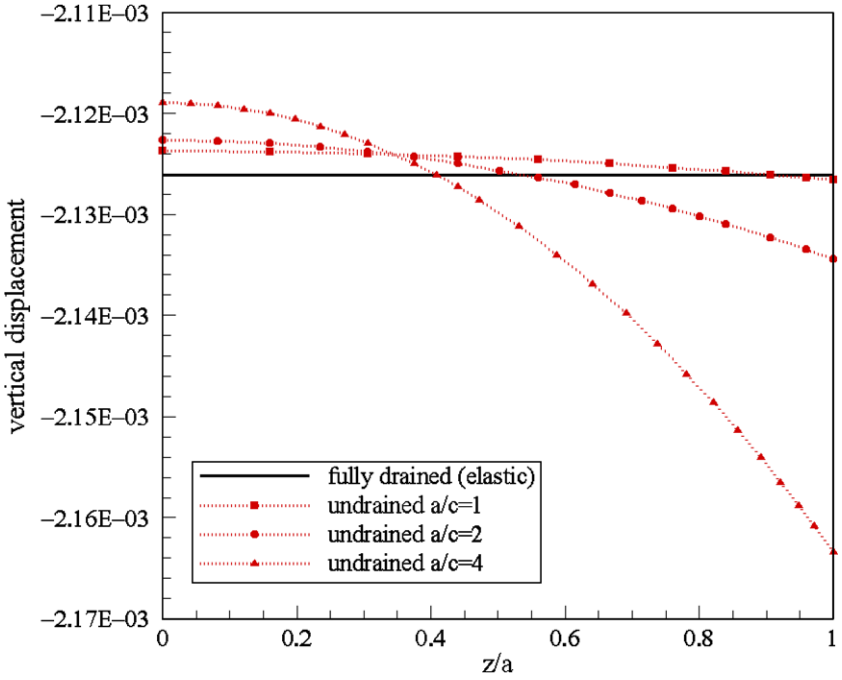

Fig. 14. Poisson effect of vertical displacement for plate bending at $x/L = 1/3,\ y/c = 0$ with $v = 0$.

effective undrained Poisson's ratio $v_u = 0.5$ when the constituents are incompressible. The vertical displacement along the z direction, as predicted by Eq. (41), is parabolic in z at $t = 0^+$. In contrast, as $t \to \infty$, when the fluid is fully drained, the system is purely elastic with $v = 0$, so the vertical displacement is invariant along the z direction as $t \to \infty$.

From Fig. 14, it is clear that as the aspect ratio a/c increases, the Poisson effect reveals itself. This explains why, for the square beam, the load relaxation solutions based on beam theory are reasonably accurate, while for a wide beam with $a/c = 4$, the comparison between the analytical solutions and FEA yields a noticeable discrepancy (*cf.* Fig. 13). For poroelasticity, the effective undrained Poisson's ratio associated with the initial stage of diffusion is usually non-vanishing, with $v_u = 0.5$ for incompressible constituents. Thus the effective Poisson's effect cannot be ignored in general when the aspect ratio a/c is large, say $a/c \geqslant 2$.

A comparison of transverse stresses along the y directions between $a/c = 1$ and $a/c = 4$ indicates that both beams have transverse stresses of similar magnitude. Therefore, the contribution of the transverse stress to the deficiency of the analytical solution for wide beams is not significant. Similarly, a comparison of transverse stress along the y directions between $L/c = 20$ and $L/c = 40$ shows that the stress patterns of the two beams are almost identical, while the magnitude of the transverse stress for the beam with $L/c = 20$ is four times larger than for the one with $L/c = 40$.

6. Practical consequences

The beam-bending method has been extensively used for measuring the permeability and mechanical properties of gels (Scherer, 1992, 1995, 1997), porous glass (Vichit-Vadakan and Scherer, 2000), cement (Valenza and Scherer, 2004; Vichit-Vadakan and

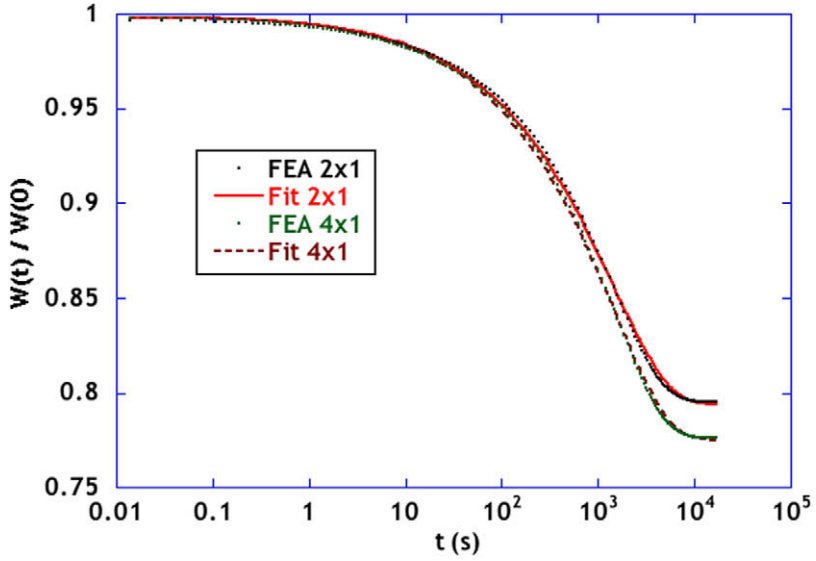

Fig. 15. Fit of approximate analytical model (curves) to output from FEA simulations (points) for plates with width/thickness ratios of 2/1 and 4/1.

Scherer, 2002, 2003), mortar (Scherer et al., 2007), and stone (Scherer and Jiménez-González, 2005), employing samples in the form of cylinders, square beams, and plates. In every case, the shape of the load relaxation curve was accurately described by the approximate theory, and the dependence of the relaxation on the viscosity and compressibility of the pore liquid was correctly captured [*e.g.*, Scherer, 1992; Vichit-Vadakan and Scherer, 2000]. It is of interest, therefore, to quantify the errors that would result in the measurement of the permeability of a porous beam, as a result of using a sample in the form of a plate. For that purpose, we have taken the load relaxation values calculated from the FEA model and treated them as experimental data to be fit to Eq. (31). The free parameters in the fit are the hydrodynamic relaxation time, τ_u, and Poisson's ratio. The fit is performed with a simplex scheme, as described in Scherer (1992) and Vichit-Vadakan and Scherer (2000). As shown in Fig. 15, the quality of the fits is excellent. The parameters returned by the fits are also in good agreement with the input parameters for FEA ($E = 1.0$ MPa, $\nu = 0.2$, $k = 1.6 \times 10^{-18}$ m^2, $\tau_u = 2.25 \times 10^4$ s): for $a/c = 2$, the fit returns $E = 0.998$ MPa, $\nu = 0.191$, $k = 1.53 \times 10^{-18}$ m^2, $\tau_u = 2.405 \times 10^4$ s; for $a/c = 4$, the fit returns $E = 0.998$ MPa, $\nu = 0.163$, $k = 1.77 \times 10^{-18}$ m^2, $\tau_u = 2.224 \times 10^4$ s. Thus, the error in permeability and Poisson's ratio would be <5% for the plate with $a/c = 2$ and <10% for $c/a = 4$, and the results for square beams would be even better. These errors are much smaller than the typical uncertainty in data obtained from conventional permeameters (Scherer et al., 2007), so the bending method using the approximate analysis is quite satisfactory for measurement of permeability, modulus, and Poisson's ratio.

7. Concluding remarks

Development of analytical solutions for bending of poroelastic beams is complicated by the presence of shear and lateral stresses, together with 3D flow. However, several of these strains and fluxes are small, so they compound the complexity of the problem, but have a relatively small quantitative impact. To capture the physics, while minimizing the mathematical difficulty, the approximate solution assumes that the basic features of simple bending theory can be adopted: (a) the only significant stress is the longitudinal bending stress; (b) the axial strain varies linearly through the thickness of the beam, and the shear strains are negligible; (c) the curvature of the beam is related to the bending moment, which varies linearly along the length of the beam, so that the vertical displacement is described by a cubic polynomial. The resulting analytical solution for the diffusion equation does not satisfy the Beltrami–Michell compatibility equations. Nevertheless, it is physically self-consistent. Moreover, it has been found to be able to capture the physics of bending of 3D poroelastic beams under three-point bending by comparisons to finite element simulations. It remains an open question to what extent the compatibility conditions can be violated without introducing severe discrepancies in the analytical solutions.

The width-to-height and length-to-height aspect ratios affect the accuracy of the analytical solutions. In particular, as the width-to-height ratio of the beam increases, the Poisson effect (*i.e.* the lateral dependence of beam flexure) becomes significant. Thus the physics of bending of the porous plate can no longer be accurately captured within the realm of beam theory. Instead, a mathematical model of the flexure of a porous body with large width-to-height ratios must be formulated based on the plate theory. Although this would certainly improve the accuracy of the result, the errors resulting from the use of beam theory are small enough so that the additional complication is rarely justified.

Acknowledgments

This work was supported by the Carbon Mitigation Initiative (CMI) project at Princeton University, sponsored by BP and Ford Motor Company.

References

Biot, M.A., 1941. General theory of three-dimensional consolidation. Journal of Applied Physics 12 (2), 155–164.
Cederbaum, G., Schulgasser, K., Li, L.P., 1998. Interesting behavior patterns of poroelastic beams and columns. International Journal of Solids and Structures 35, 4931–4943.
Chen, A.T.F., 1966. Plane Strain and Axisymmetric Primary Consolidation of Saturated Clays, Ph.D. Thesis, RPI (advisor: Robert L. Schiffman), New York.
Cheng, A.H.D., 1998. On generalized plane strain poroelasticity. International Journal of Rock Mechanics and Mining Sciences 35 (2), 183–193.
Corfdir, A., Dormieux, L., 1998. Mathematical model of flexure in a saturated geological layer: application to faulting. Tectonophysics 292, 267–278.
Coussy, O., 2004. Poromechanics. Wiley, West Sussex, England.
Cryer, C.W., 1963. A comparison of the three-dimensional consolidation theories of Biot and Terzaghi. Quarterly Journal of Mechanics and Applied Mathematics 16 (4), 401–412.
Detournay, E., Cheng, A.H.D., 1994. Fundamentals of poroelasticity. In: Hudson, J. (Ed.), Comprehensive Rock Engineering. Pergamon Press.
Kameo, Y., Adachi, T., Hojo, M., 2008. Transient response of fluid pressure in a poroelastic material under uniaxial cyclic loading. Journal of the Mechanics and Physics of Solids 56 (5), 1794–1805.
Li, L.P., Schulgasser, K., Cederbaum, G., 1995. Theory of poroelastic beams with axial diffusion. Journal of the Mechanics and Physics of Solids 43 (12), 2023–2042.
Mandel, J., 1953. Consolidation des sols (Etude mathématique). Géotechnique 3, 287–299.
Manfredini, P., Cocchetti, G., Maier, G., Redaelli, A., Montevecchi, F.M., 1999. Poroelastic finite element analysis of a bone specimen under cyclic loading. Journal of Biomechanics 32 (2), 135–144.
Nowinski, J.L., Davis, C.F., 1972. The flexure and torsion of bones viewed as anisotropic poroelastic bodies. International Journal of Engineering Science 10 (12), 1063–1079.
Popov, E.P., 1968. Introduction to Mechanics of Solids. Prentice-Hall, Englewood Cliffs, NJ.
Prévost, J.H., 1981. Dynaflow – User's Manual, Princeton University, NJ (updated 2009).
Rice, J.R., Cleary, M.P., 1976. Some basic stress diffusion solutions for fluid-saturated elastic porous media with compressible constituents. Reviews of Geophysics and Spaces Physics 14 (2), 227–241.
Scherer, G.W., 1992. Bending of gel beams: methods for characterizing elastic properties and permeability. Journal of Non-Crystalline Solids 142, 18–35.
Scherer, G.W., 1995. Viscoelasticity and permeability of silica gels. Faraday Discussions 101, 225–234.
Scherer, G.W., 1996. Bending of gel beams: effect of deflection rate and Hertzian indentation. Journal of Non-Crystalline Solids 201, 1–25.
Scherer, G.W., 1997. Effect of drying on properties of silica gel. Journal of Non-Crystalline Solids 215, 155–168.
Scherer, G.W., 2000. Measuring permeability of rigid materials by a beam-bending method: I, theory. Journal of the American Ceramic Society 83 (9), 2231–2239. Erratum 87 (2004) 1612–1613.
Scherer, G.W., 2004. Measuring permeability of rigid materials by a beam-bending method: IV transversely isotropic plate. Journal of the American Ceramic Society 87 (8), 1517–1524.
Scherer, G.W., Jiménez-González, I., 2005. Characterization of swelling in clay-bearing stone. In: Turkington, A.V. (Ed.), Stone Decay and Conservation SP-390. Geological Society of America, pp. 51–61.
Scherer, G.W., Valenza II, J.J., Simmons, G., 2007. New methods to measure liquid permeability in porous materials. Cement and Concrete Research 37 (3), 386–397.
Skempton, A.W., 1954. The pore-pressure coefficients A and B. Geotechnique 4, 143–147.
Taber, L.A., 1992. A theory for transverse deflection of poroelastic plates. Journal of Applied Mechanics – Transactions of the ASME 59 (3), 628–634.
Thomas, H.R., Zhou, Z., 1997. Minimum time-step size for diffusion problem in FEM analysis. International Journal for Numerical Methods in Engineering 40 (20), 3865–3880.
Timoshenko, S.P., 1940. Theory of Plates and Shells. McGraw-Hill Inc., New York.
Truty, A., Zimmermann, T., 2006. Stabilized mixed finite element formulations for materially nonlinear partially saturated two-phase media. Computer Methods in Applied Mechanics and Engineering 195, 1517–1546.
Valenza II, J.J., Scherer, G.W., 2004. Measuring permeability of rigid materials by a beam-bending method: V. Isotropic rectangular plates of cement paste. Journal of the American Ceramic Society 87 (10), 1927–1931.

Vichit-Vadakan, W., Scherer, G.W., 2000. Measuring permeability of rigid materials by a beam-bending method: II. Porous vycor. Journal of the American Ceramic Society 83 (9), 2240–2245. Erratum 87 (2004) 1614.

Vichit-Vadakan, W., Scherer, G.W., 2002. Measuring permeability of rigid materials by a beam-bending method: III. Cement paste. Journal of the American Ceramic Society 85 (6), 1537–1544. Erratum 87 (8) (2004) 1615.

Vichit-Vadakan, W., Scherer, G.W., 2003. Measuring permeability and stress relaxation of young cement paste by beam-bending. Cement and Concrete Research 33 (12), 1925–1932.

Vermeer, P.A., Verruijt, A., 1981. An accuracy condition for consolidation by finite elements. International Journal for Numerical and Analytical Methods in Geomechanics 5 (1), 1–14.

Wang, Z.H., Prévost, J.H., Coussy, O., 2009. Bending of fluid saturated poroelastic beams with compressible constituents. International Journal for Numerical and Analytical Methods in Geomechanics 33, 425–447.

Zhang, D., Cowin, S.C., 1994. Oscillatory bending of a poroelastic beam. Journal of the Mechanics and Physics of Solids 42 (10), 1575–1599.